Supporting Information

Enhancing Pancreatic Cancer Ablation Efficiency:

Bipolar IRE with Conductive MOF

Lei Xu,‡[a,b,d] Wenjing Lou,‡[a] Fan Xu,‡[a] Yujiao Xie,[d,e] Yue Hu,[d,e] Liting Xie,[a] Chengyue Zhang,[a] Aochi Liu,[d,e] Xinyu Miao,[d,e] Zhiwei Hou,[d,e] Wenyuan Ma,[a] QiYu Zhao,*[a,c] Jie Lin,*[d,e] Aiguo Wu,*[d,e] Tianan Jiang*[a,c]

a Department of Ultrasound Medicine, The First Affiliated Hospital, Zhejiang University School of Medicine, Hangzhou, Zhejiang 310000, P.R. China

b Department of Ultrasound Medicine, Affiliated Jinhua Hospital Zhejiang University School of Medicine, Jinhua, Zhejiang 321000, P.R. China

c Zhejiang University Cancer Center, Hangzhou, Zhejiang 310000, P.R. China

d Ningbo Key Laboratory of Biomedical Imaging Probe Materials and Technology, Laboratory of Advanced Theranostic Materials and Technology, Chinese Academy of Sciences (CAS) Key Laboratory of Magnetic Materials and Devices, Ningbo Institute of Materials Technology and Engineering, Chinese Academy of Sciences, Ningbo 315201, China

e Zhejiang International Cooperation Base of Biomedical Materials Technology and Application, Zhejiang Engineering Research Center for Biomedical Materials, Ningbo Cixi Institute of Biomedical Engineering, Ningbo 315300, China

** Corresponding author e-mail addresses: tiananjiang@zju.edu.cn (T. Jiang), aiguo@nimte.ac.cn (A. Wu), linjie@nimte.ac.cn (J. Lin), zhaoqiyu2000@zju.edu.cn (Q. Zhao).*

‡ *These authors contributed equally to this work.*

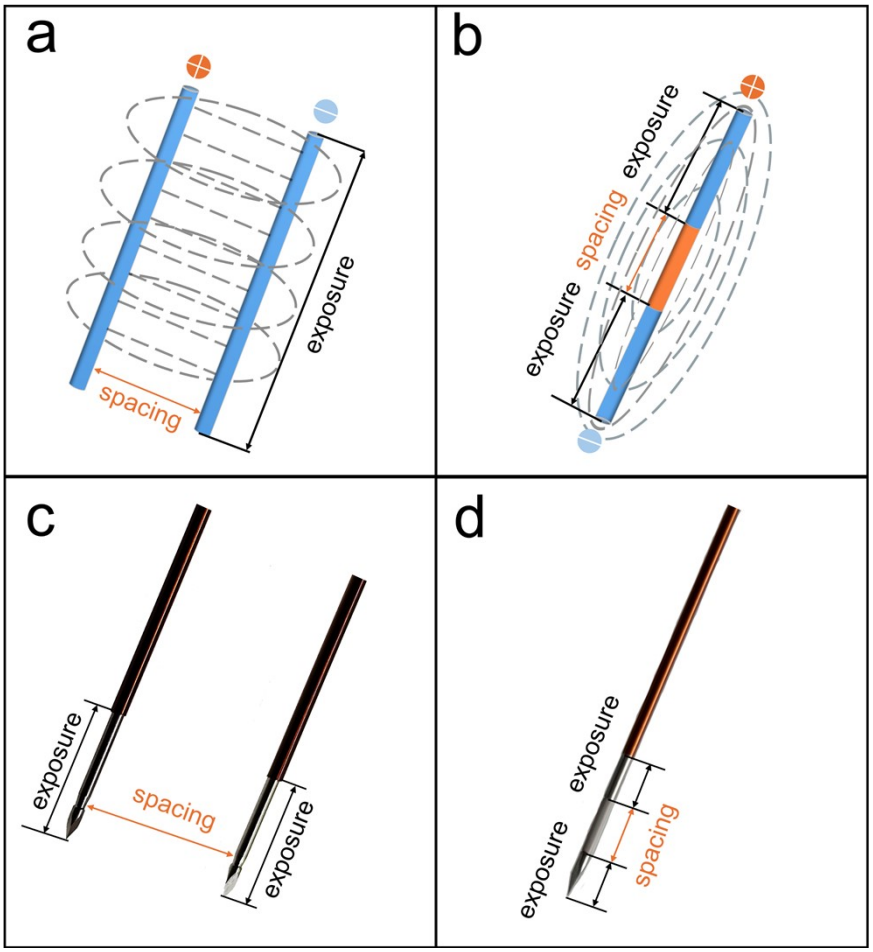

Fig. S1 Design model figure and real product figure of monopolar and bipolar electrode. Design drawing (a) and real product (c) for the monopolar electrode; design drawing (b) and real product (d) for the bipolar electrodes. The grey dashed lines represent the simulated electric field range and shape of the monopolar and bipolar electrodes, respectively.

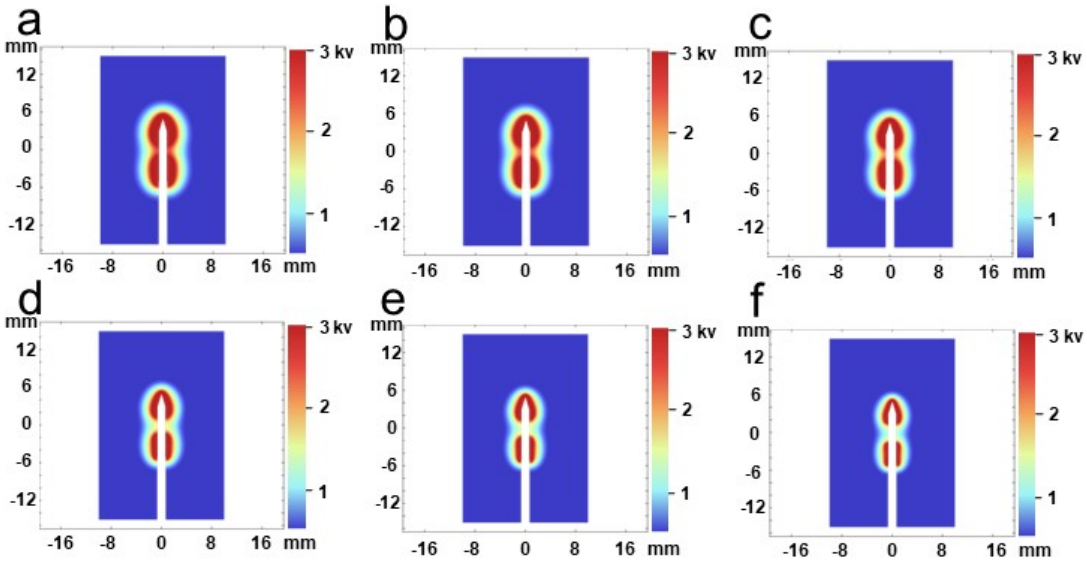

Fig. S2 COMSOL Multiphysics software simulation of the bipolar electrodes electric field distribution parallel to the electrodes at the electric field strengths of 2750 V/cm (a), 2500 V/cm (b), 2250 V/cm (c), 1750 V/cm (d), 1500 V/cm (e), and 1250 V/cm (f), respectively.

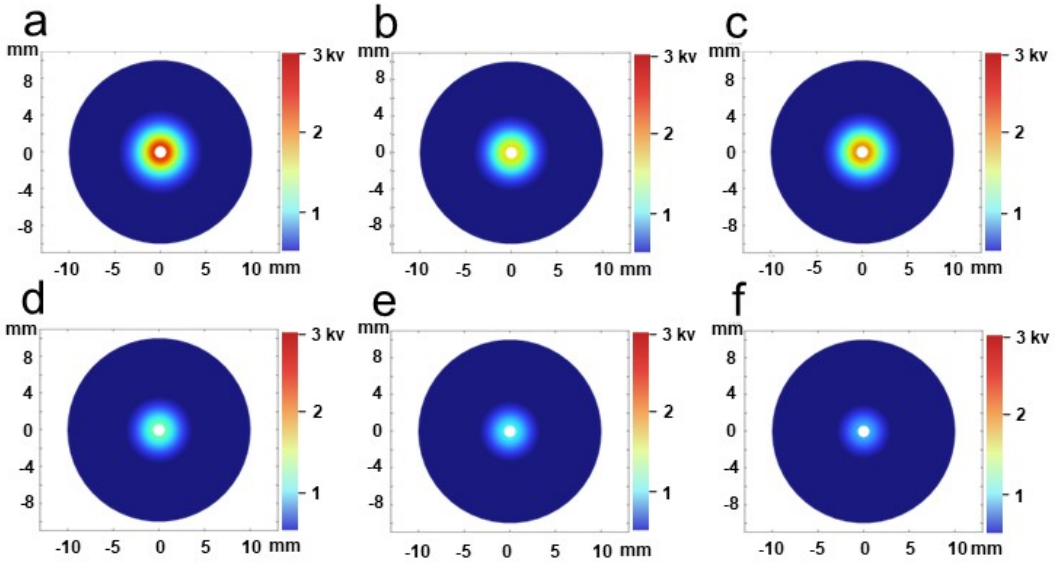

Fig. S3 COMSOL Multiphysics software simulation of the bipolar electrodes electric field distribution parallel to the electrodes at the electric field strengths of 2750 V/cm (a), 2500 V/cm (b), 2250 V/cm (c), 1750 V/cm (d), 1500 V/cm (e), and 1250 V/cm (f), respectively.

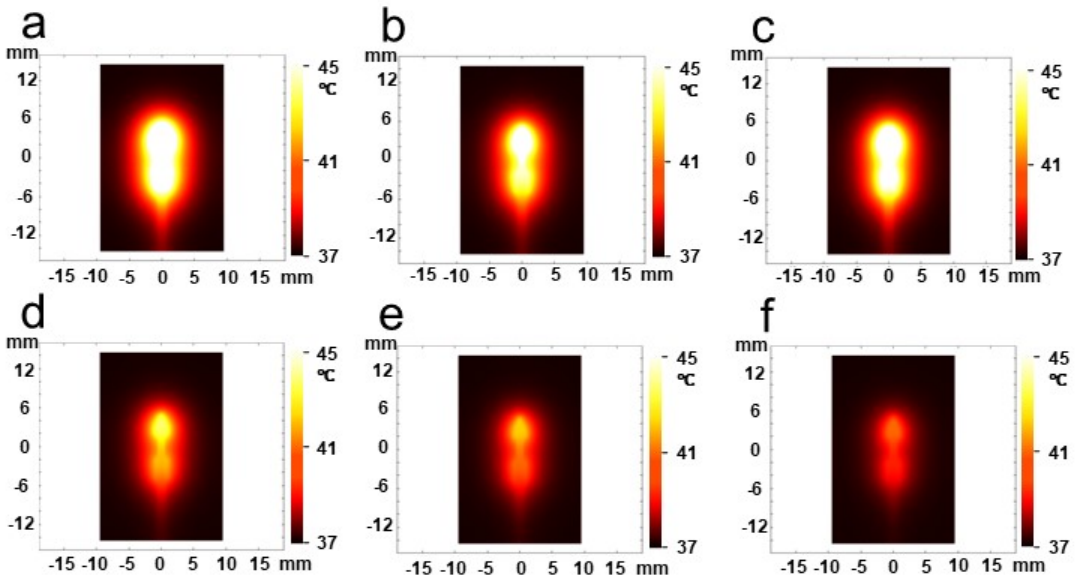

Fig. S4 COMSOL Multiphysics software simulation of the bipolar electrodes ablation temperature distribution at the electric field strengths of 2750 V/cm (a), 2500 V/cm (b), 2250 V/cm (c), 1750 V/cm (d), 1500 V/cm (e), and 1250 V/cm (f), respectively.

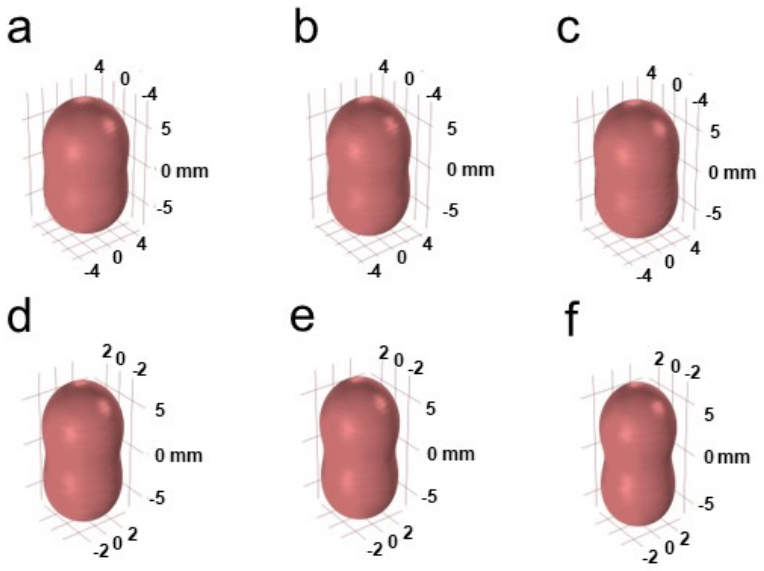

Fig. S5 COMSOL Multiphysics software simulation of the bipolar electrodes ablation volume at the electric field strengths of 2750 V/cm (a), 2500 V/cm (b), 2250 V/cm (c), 1750 V/cm (d), 1500 V/cm (e), and 1250 V/cm (f), respectively.

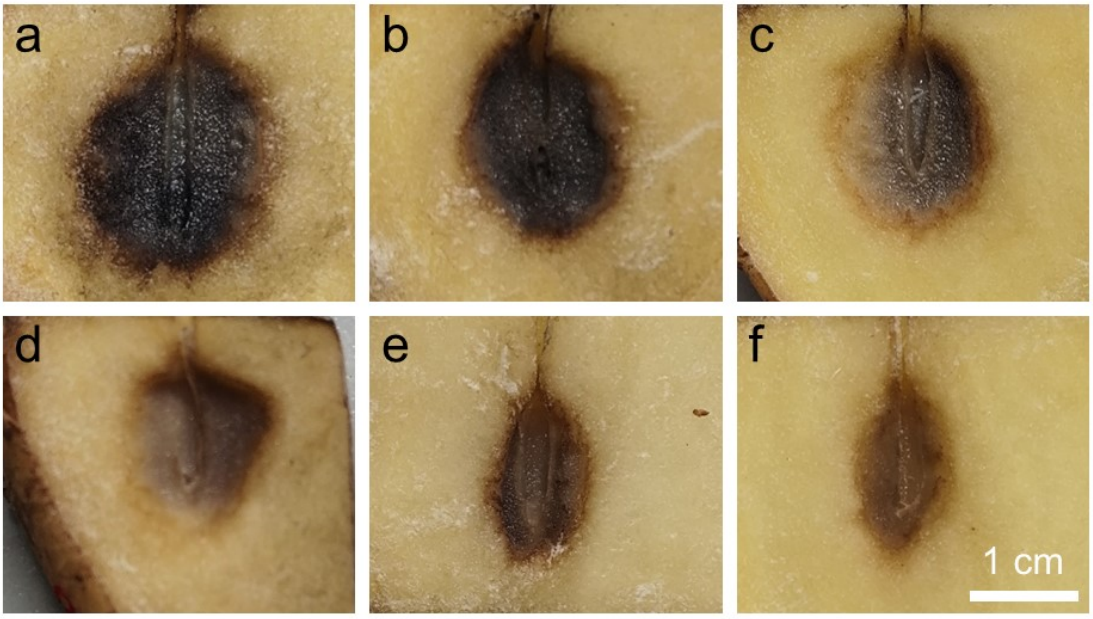

Fig. S6 Potato ablation model evaluating the ablation effect and range of bipolar electrodes at field strengths of 3000 V/cm (a), 2500 V/cm (b), 2000 V/cm (c), 1500 V/cm (d), 1000 V/cm (e), and 750 V/cm (f), respectively.

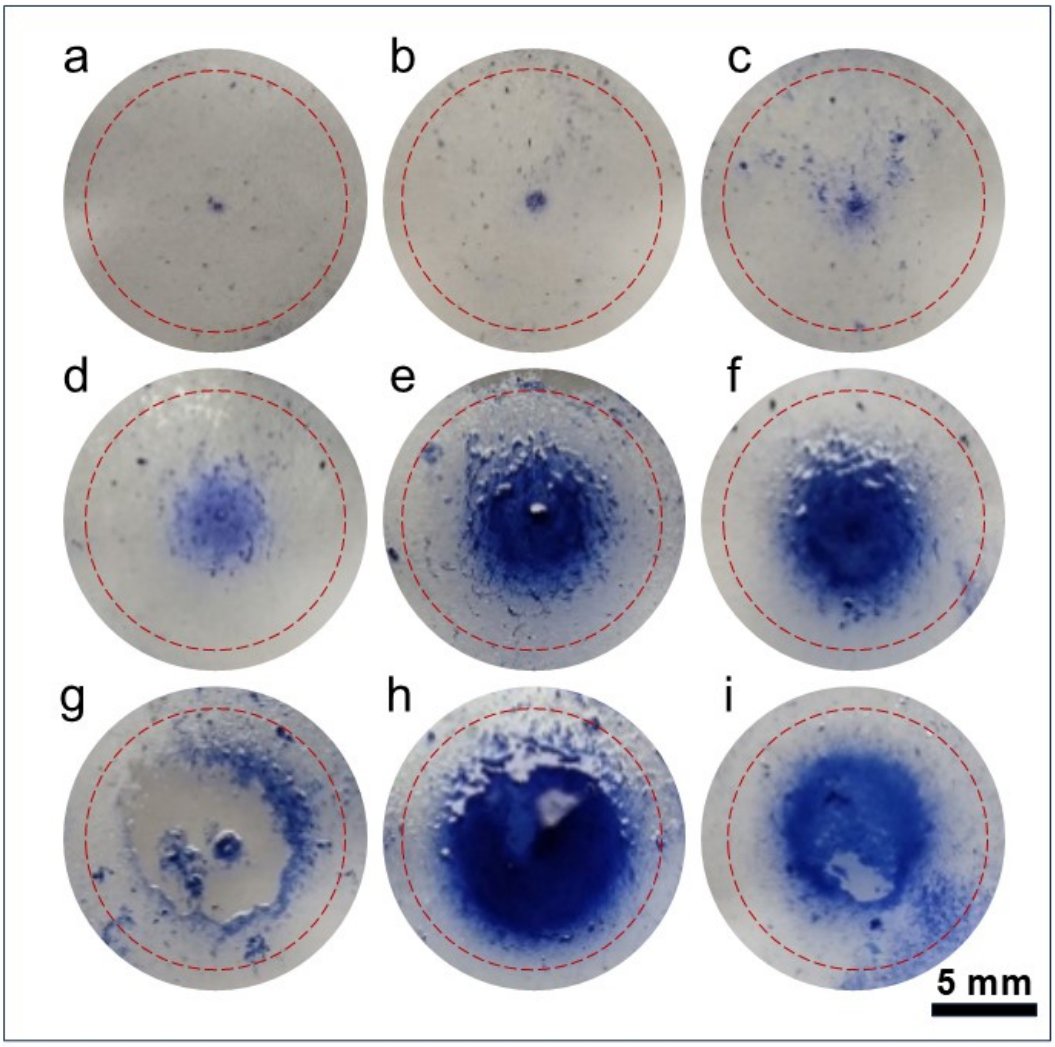

Fig. S7 Cell Trypan Blue assay evaluating the killing ability of pancreatic tumor cells using bipolar electrodes ablation at field strengths of 750 V/cm (a), 1000 V/cm (b), 1250 V/cm (c), 1500 V/cm (d), 1750 V/cm (e), 2000 V/cm (f), 2250 V/cm (g), 2500 V/cm (h), and 2750 V/cm (i), respectively.

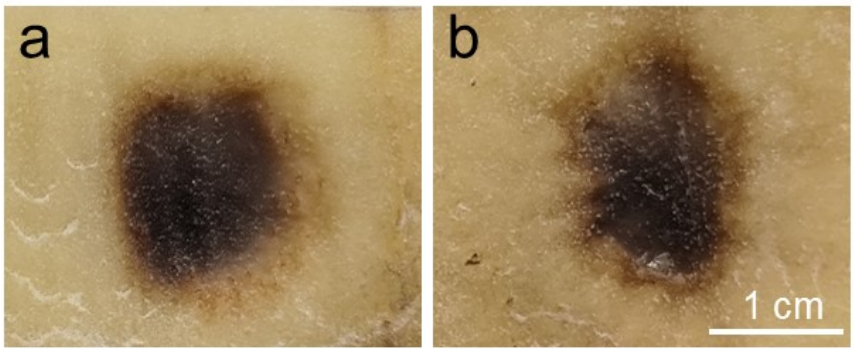

Fig. S8 Comparison of the ablation zones in the potato model: (a) monopolar electrode at 1500 V/cm and (b) bipolar electrodes at 2500 V/cm.

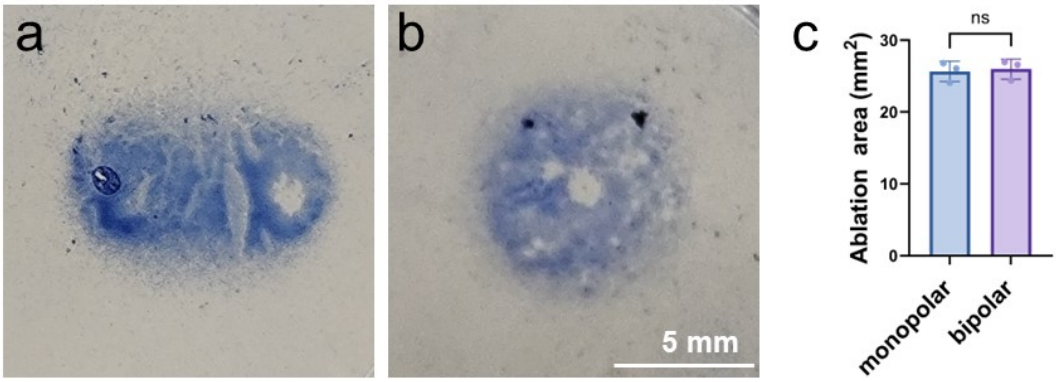

Fig. S9 Comparison of the IRE ablation zones in the cell Trypan Blue assay: (a) monopolar electrode at 1500 V/cm; (b) bipolar electrodes at 2500 V/cm; (c) Semi-quantitative analysis of the ablation ranges of monopolar electrode at a field intensity of 1500 V/cm and bipolar. electrodes at 2500 V/cm. “ns” means no statistical significance.

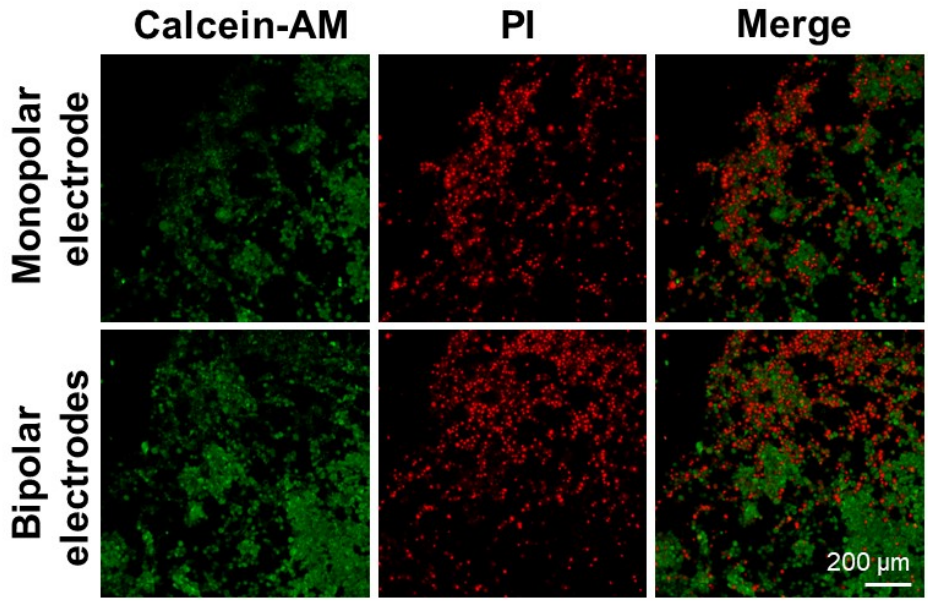

Fig. S10 Live/dead staining of KPC cell treatment with monopolar electrode ablation at 1500 V/cm and bipolar electrodes ablation at 2500 V/cm.

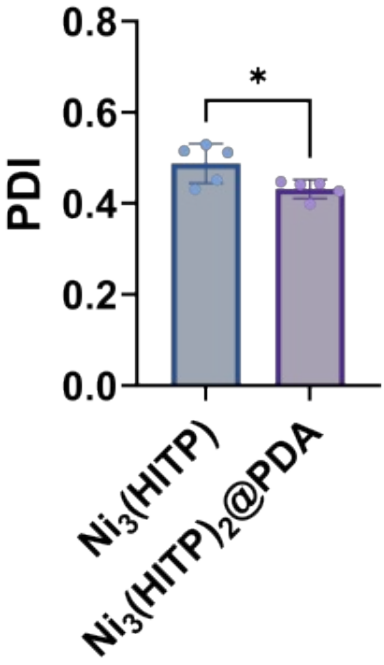

Fig. S11 Polymer dispersity index of $Ni_3(HITP)_2$ and $Ni_3(HITP)_2$@PDA, statistical significance is indicated as * $p < 0.05$.

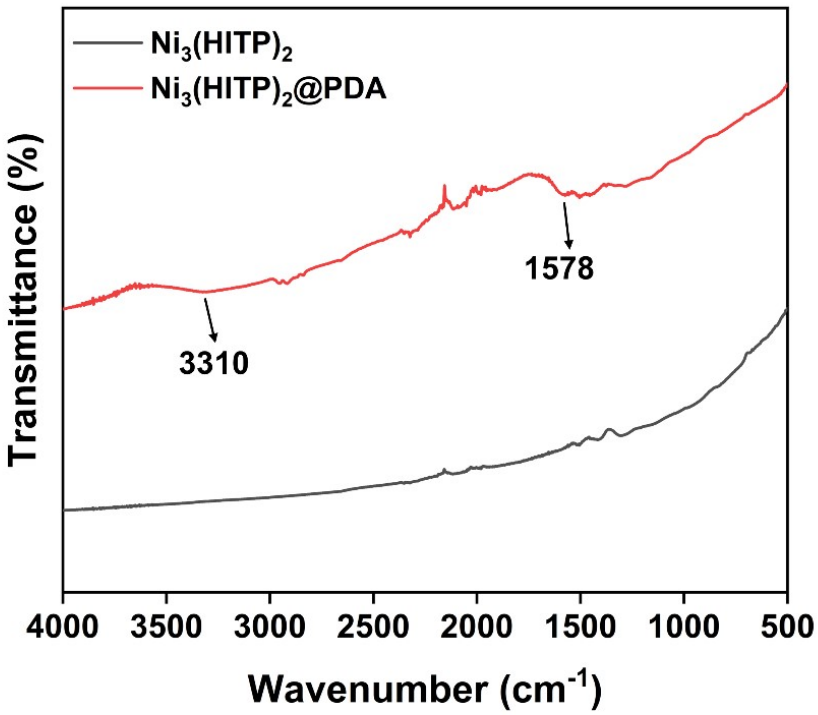

Fig. S12 FT-IR spectra of $Ni_3(HITP)_2$ and $Ni_3(HITP)_2$@PDA

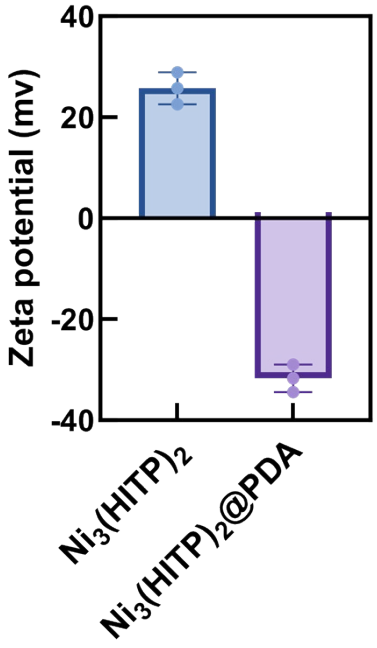

Fig. S13 Zeta potential of $Ni_3(HITP)_2$ and $Ni_3(HITP)_2$@PDA.

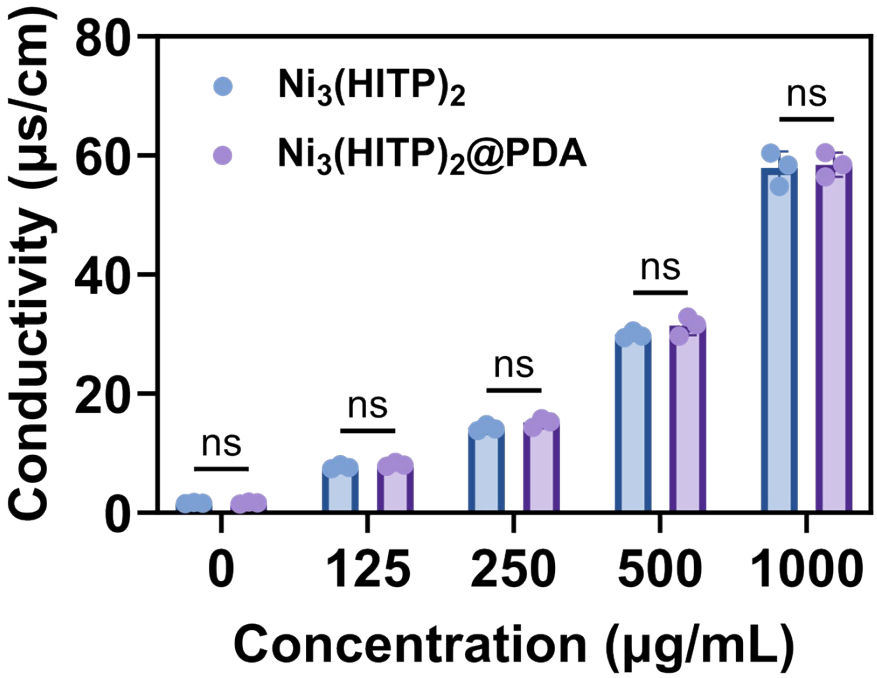

Fig. S14 Conductivity of aqueous solutions with different concentrations of $Ni_3(HITP)_2$ and $Ni_3(HITP)_2$@PDA. ns means no significant difference. “ns” means no significant difference.

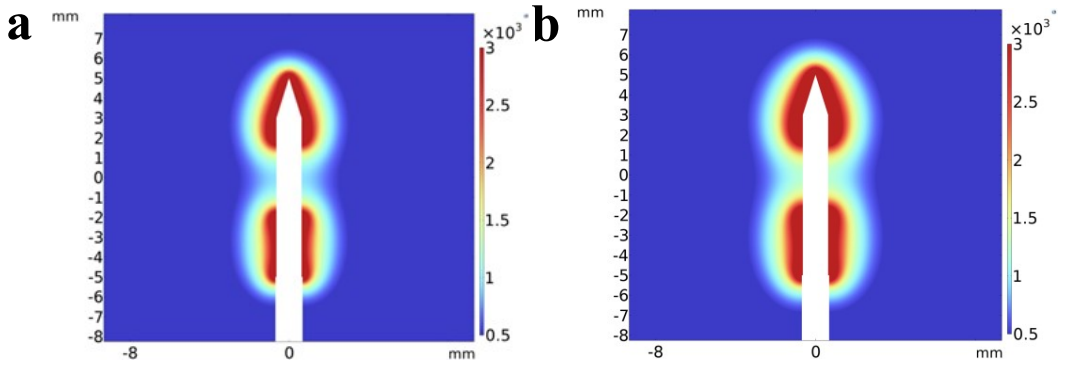

Fig. S15 Schematic diagram of simulated electric field distribution. (a) Bipolar electrode ablation electric field distribution area; (b) Bipolar electrode combined $Ni_3(HITP)_2$@PDA ablation electric field distribution area.

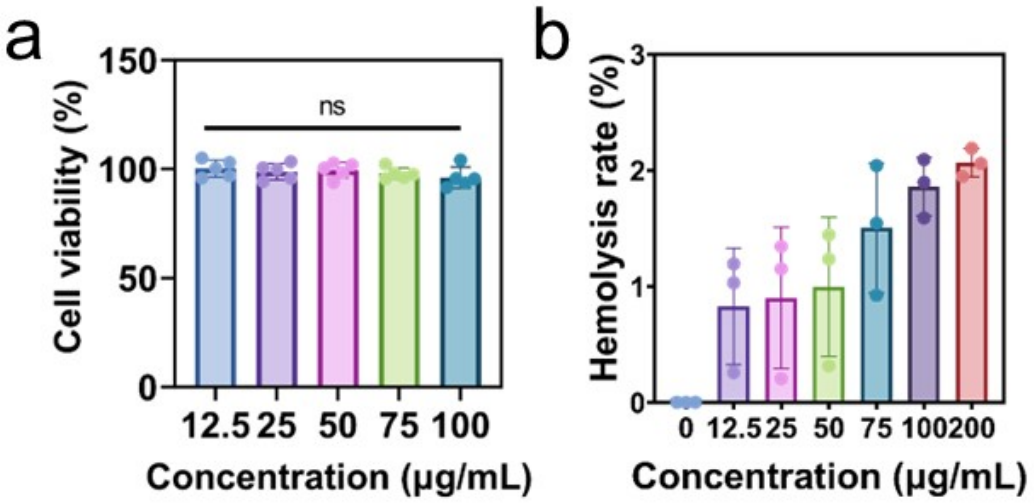

Fig. S16 (a) Cytotoxicity of different concentrations of $Ni_3(HITP)_2$@PDA after 12 hours of co-incubation. ns indicated no statistical significance. "ns" means no significant difference. (b) Different concentrations of $Ni_3(HITP)_2$@PDA hemolysis experiment.

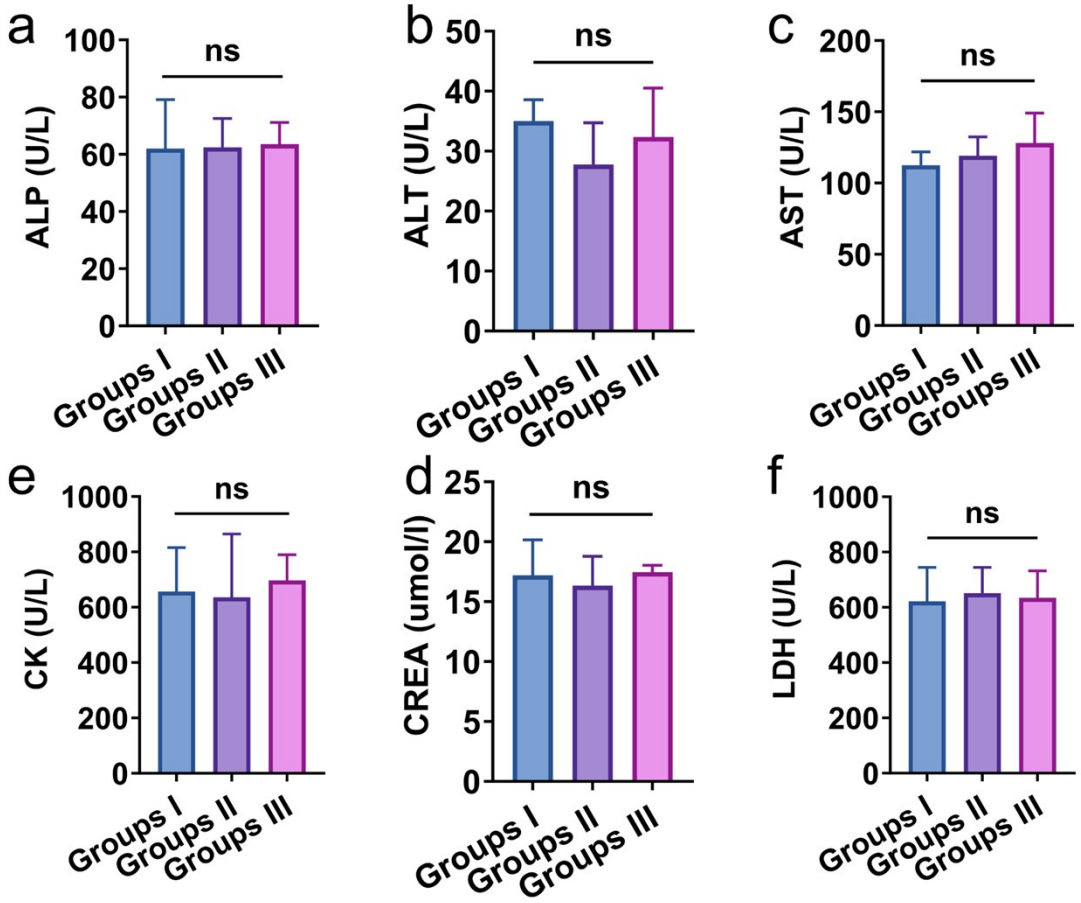

Fig. S17 Blood biochemical test results of mice in different treatment groups, including ALP (a), ALT (b), AST (c), CK (e), CREA (d), and LDH (f) staining. “ns” means no significant difference. Groups I, II and III represent the Control, Bipolar Electrodes and Bipolar Electrodes +$Ni_3(HITP)_2$@PDA, respectively. The bipolar electrodes parameters: pulse intensity = 2500 V/cm; pulse duration = 90 μs; number of pulses = 90.

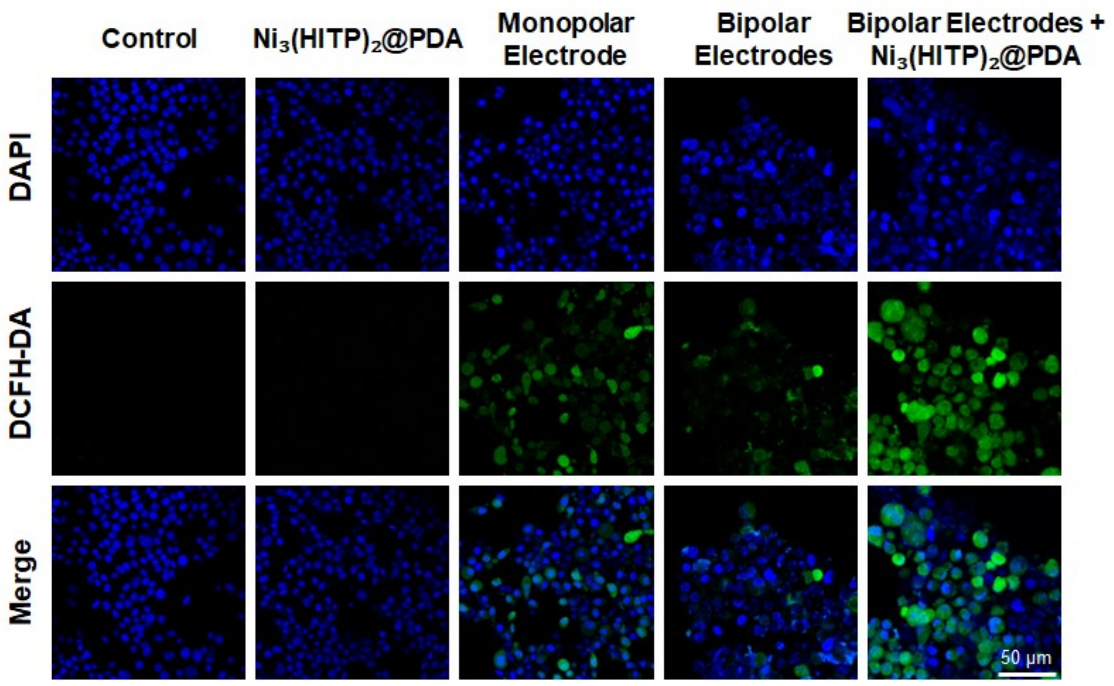

Fig. S18 ROS staining of control, $Ni_3(HITP)_2$@PDA, monopolar electrode, bipolar electrodes and bipolar electrodes+ $Ni_3(HITP)_2$@PDA groups. The monopolar electrodes parameters: pulse intensity = 1500 V/cm; pulse duration = 90 μs; number of pulses = 90; bipolar electrodes parameters: pulse intensity = 2500 V/cm; pulse duration = 90 μs; number of pulses = 90.

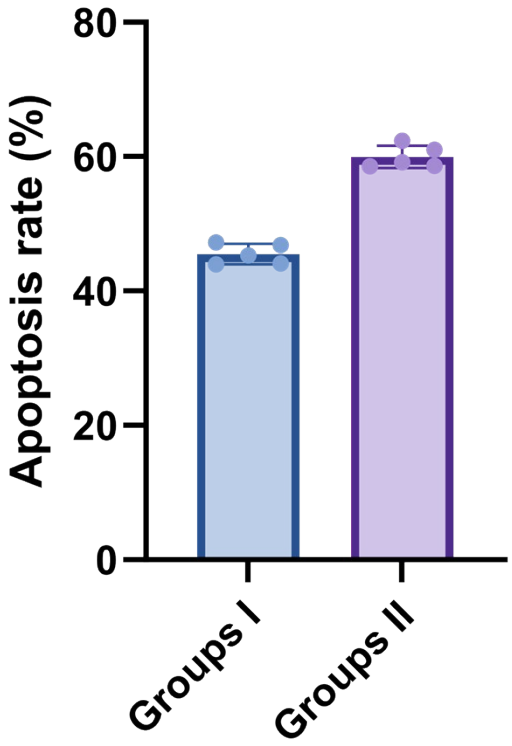

Fig. S19 Apoptosis rates of tumor cells under different treatment conditions, as analyzed by flow cytometry. Groups I and II correspond to the Bipolar Electrodes group and the Bipolar Electrodes + $Ni_3(HITP)_2$@PDA group, respectively.

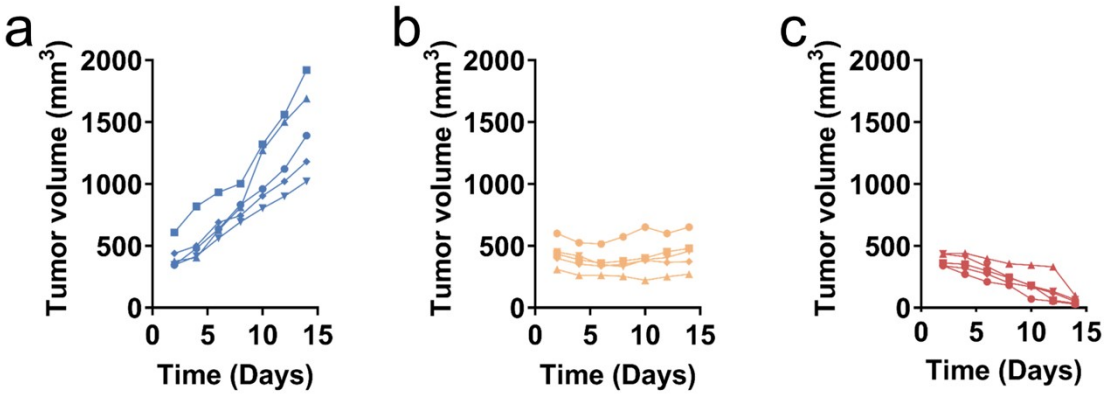

Fig. S20 Tumor volume changes in different groups 14 days after treatment in the Control (a), Bipolar Electrodes (b), and Bipolar Electrodes + $Ni_3(HITP)_2$@PDA (c) groups. The bipolar electrodes parameters: pulse intensity = 2500 V/cm; pulse duration = 90 μs; number of pulses = 90.

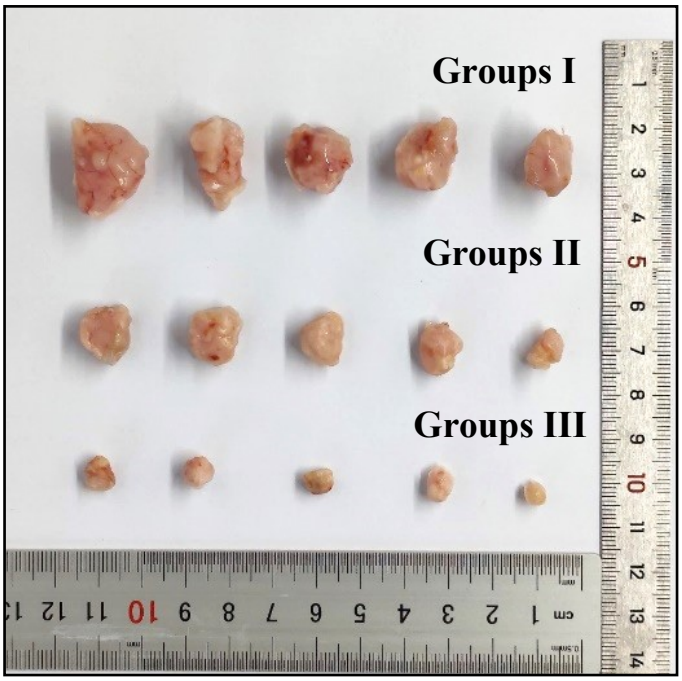

Fig. S21 Photographs of the isolated tumors on day 14. Groups I, II, and III represent the Control, Bipolar Electrodes and Bipolar Electrodes +$Ni_3(HITP)_2$@PDA groups, respectively.

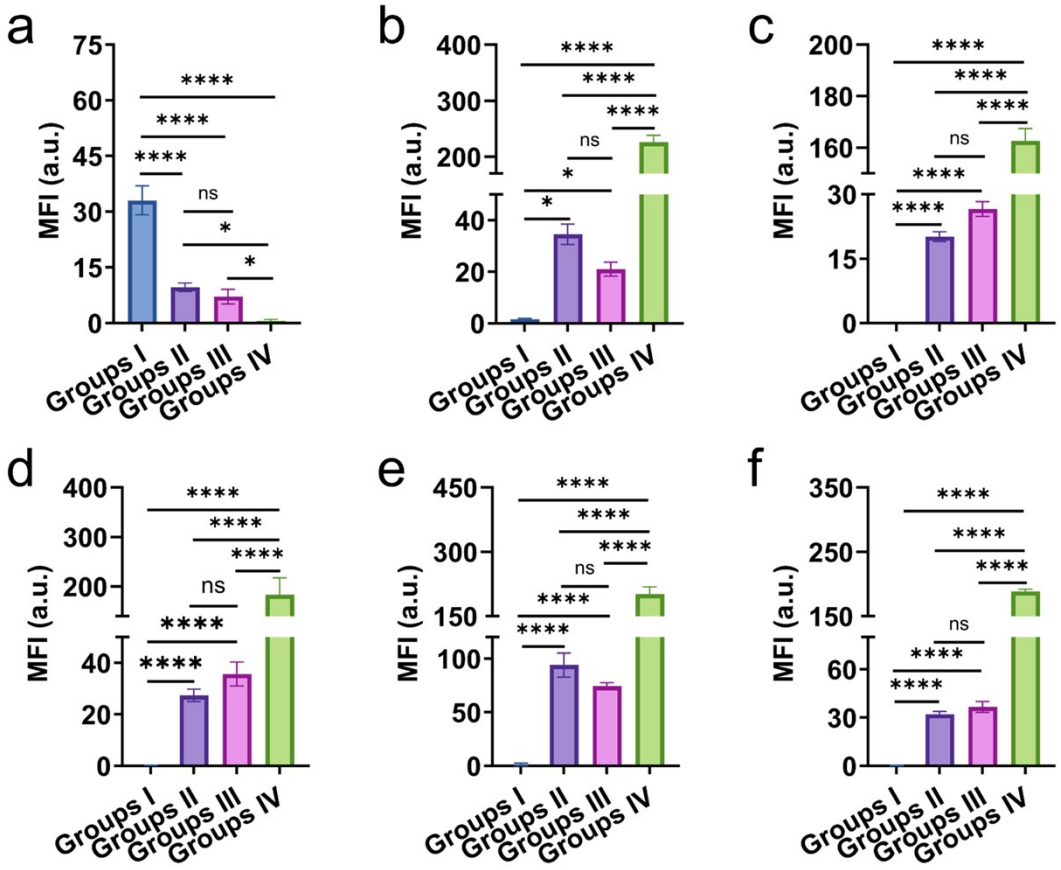

Fig. S22 Quantification of immunofluorescence intensities for Ki67 (a), Tunel (b), P53 (c), BAX (d), BCL-2 (e) and TNF-α (f) staining across different groups. Statistical significance is indicated as * $p < 0.05$, **** $p < 0.0001$, and "ns" means no significant difference. Groups I, II, III and IV represent the Control, Monopolar Electrode, Bipolar Electrodes and Bipolar Electrodes +$Ni_3(HITP)_2$@PDA, respectively. The monopolar electrodes parameters: pulse intensity = 1500 V/cm; pulse duration = 90 μs; number of pulses = 90; bipolar electrodes parameters: pulse intensity = 2500 V/cm; pulse duration = 90 μs; number of pulses = 90.